JOC Article
pubs.acs.org/joc

Importance of Equilibrium Fluctuations between Most Stable Conformers in the Control of the Reaction Mechanism

Bruno S. Souza and Faruk Nome*

Departamento de Química, Universidade Federal de Santa Catarina, Florianópolis, Santa Catarina 88040-900, Brazil

faruk@qmc.ufsc.br

Received July 12, 2010

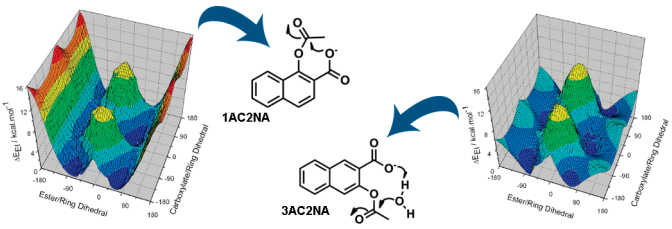

Hydrolysis of closely related compounds show how subtle structural differences markedly change reaction mechanisms. While in the hydrolysis of 3-acetoxy-2-naphthoic acid (**3AC2NA**) the reacting groups rotate freely, favoring intramolecular general base catalysis, the 1-acetoxy-2-naphthoic acid (**1AC2NA**) isomer is caged in an energy wall that freezes a conformation suitable for intramolecular nucleophilic attack, in contrast to the results expected for reactions governed largely by electronic effects. The results highlight the importance of the dynamics of equilibrium fluctuations between most stable conformers in the control of the reaction mechanism, (i) promoting the nucleophilic attack in **1AC2NA** by allowing the most stable conformers to equilibrate only via rotation in a direction that intercepts the reaction coordinate and (ii) favoring a general base-catalyzed water attack in **3AC2NA** by favoring equilibration via rotation that allows inclusion of a water molecule in a proper position for reaction.

Introduction

Hydrolyses of acetyl salicylic acid (aspirin) and its derivatives are classical examples of intramolecular catalysis.[1] In the pH-independent region of rate constants, the carboxylate group acts either as a general base or as a nucleophile, and this behavior is highly dependent on electronic effects.[2] In the parent compound the carboxylate group is a general base catalyst, whereas in the hydrolysis of the 3,5-dinitro derivative it is a nucleophile forming a salicylic anhydride intermediate (Scheme 1). To explain this behavior, Fersht and Kirby proposed that the tetrahedral intermediates involved in the nucleophilic attack revert to reagents when the leaving group ability is relatively low, as with aspirin. In the highly activated acetyl 3,5-dinitro salicylic acid the nucleophilic path is favored as a result of the similar pK_a' values of the leaving group and nucleophile.[2b]

SCHEME 1. Suggested Mechanisms for Decomposition of the Acetyl Salicylates According to References 1 and 2

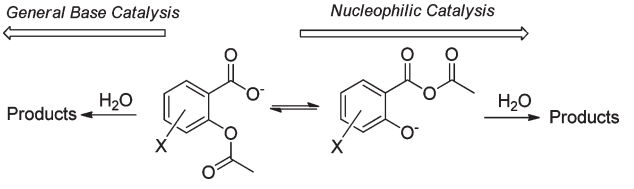

These observations are consistent with those of Gold et al.,[3] who showed that intermolecular nucleophilic catalysis by acetate ion is observed in the hydrolysis of acetate esters of strongly acidic phenols, such as 2,4- and 2,6-dinitrophenol, with formation of acetic anhydride. Conversely, the hydrolysis of phenyl and *p*-methylphenyl acetates are subject solely to general base catalysis. It was proposed that nucleophilic attack by the acetate group occurs only for esters whose

(1) (a) Fersht, A. R.; Kirby, A. J. *J. Am. Chem. Soc.* **1967**, *89*, 5960–5961. (b) Fersht, A. R.; Kirby, A. J. *J. Am. Chem. Soc.* **1967**, *89*, 5961–5962.
(2) (a) Fersht, A. R.; Kirby, A. J. *J. Am. Chem. Soc.* **1967**, *89*, 4857–4863. (b) Fersht, A. R.; Kirby, A. J. *J. Am. Chem. Soc.* **1968**, *90*, 5818–5826. (c) Fersht, A. R.; Kirby, A. J. *J. Am. Chem. Soc.* **1968**, *90*, 5826–5832.

(3) Gold, V.; Oakenful., Dg; Riley, T. *J. Chem. Soc. B* **1968**, 515–519.

Published on Web 10/08/2010 DOI: 10.1021/jo101366m

SCHEME 2. Proposed Mechanism for Hydrolysis of the Phosphodiester BMIPP, Involving Intramolecular General Acid Catalysis by the Imidazolium Group and Nucleophilic Catalysis by the Imidazole Free Base

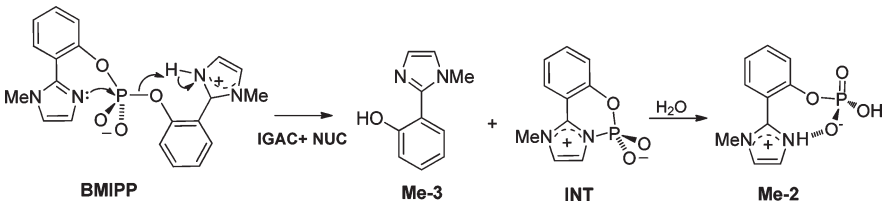

leaving group pK_a' is less than 3 units higher than that of acetic acid.[3]

Recently, we reported a complete mechanistic study for the hydrolysis of **BMIPP** (bis(2-(1-methyl-1*H*-imidazolyl)-phenyl) phosphate), which like enzyme active sites deploying two histidines has two catalytic groups in potentially productive proximity of the unreactive phosphodiester center.[4] We have found that **BMIPP** is hydrolyzed nearly 10^{11} times faster than expected for diphenyl phosphate. The significant combined effect of the two catalytic groups was explained in terms of two factors: (i) an initial step that includes intramolecular nucleophilic catalysis (NUC) by the neighboring imidazole free base, concerted with (ii) the expected efficient intramolecular general acid catalysis (IGAC). Taken together, factors i and ii result in the formation of the arylimidazole **Me-3** and a phosphorane intermediate (**INT**), which decomposes to the phosphate monoester **Me-2** (Scheme 2).[4]

In the absence of a steric or stereoelectronic barrier, intramolecular nucleophilic catalysis is reliably more efficient than intramolecular general base catalysis (IGBC), with effective molarities of up to 10^9 in conformationally flexible systems, compared with a limit of about 60 M for IGBC,[5] and this limit applies in particular to all known model systems involving water as the primary nucleophile.

Intramolecular reactions depend on the spatial relationship of the reacting groups and time spent at the critical reaction distance.[6] To explore the importance of steric and conformational effects in these well-known intramolecular reactions, we examined hydrolysis in two structurally related compounds, namely, 1-acetoxy-2-naphthoic acid (**1AC2NA**) and 3-acetoxy-2-naphthoic acid (**3AC2NA**). Despite the apparently similar stereochemistry of **1AC2NA** and **3AC2NA**, the carboxylate groups of the two esters catalyze hydrolysis via completely different mechanisms.

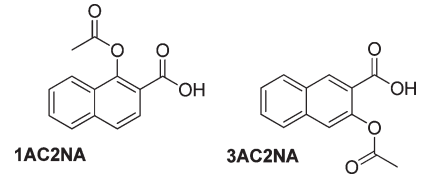

Results and Discussion

Kinetics. pH−rate profiles for the hydrolysis of 1-acetoxy-2-naphthoic acid (**1AC2NA**) and 3-acetoxy-2-naphthoic acid (**3AC2NA**) are similar at 45.0 °C (Figure 1) and of the same

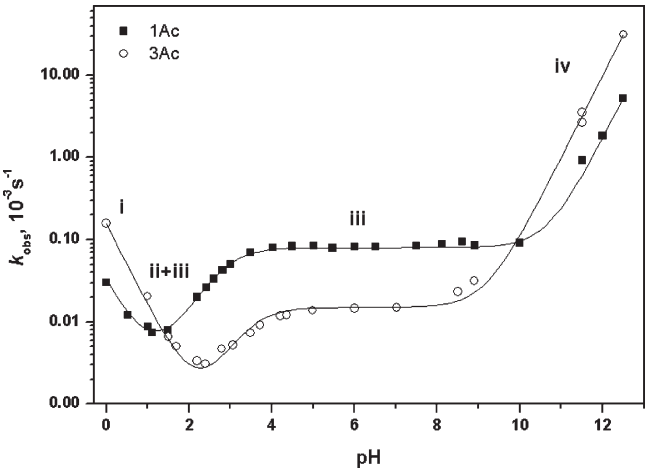

FIGURE 1. pH−rate profile for hydrolyses of **1AC2NA** (black squares) and **3AC2NA** (open circles) at 45.0 °C and μ = 1 M (KCl). The solid lines represent fits to the experimental data using eq 1. Regions i, ii + iii, iii, and iv were marked to indicate the main reactions contributing to k_{obs}, as defined in Scheme 3.

SCHEME 3. Proposed Reactions for Hydrolyses of 1AC2NA and 3AC2NA, Involving Intramolecular Catalysis (Paths ii and iii) and Specific Acid- and Base-Catalyzed Reactions (Paths i and iv)

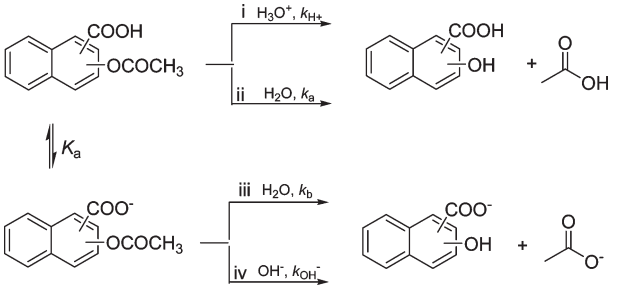

form as that of aspirin[2c] hydrolysis. Kinetic data for both compounds are consistent with Scheme 3, allowing derivation of eq 1.

$$k_{obs} = k_{H^+}[H]^+ + k_{OH^-}[OH]^- + k_a\left(\frac{10^{-pH}}{10^{-pH}+K_a}\right) + k_b\left(\frac{K_a}{10^{-pH}+K_a}\right) \quad (1)$$

(4) Orth, E. S.; Brandao, T. A. S.; Souza, B. S.; Pliego, J. R.; Vaz, B. G.; Eberlin, M. N.; Kirby, A. J.; Nome, F. *J. Am. Chem. Soc.* **2010**, *132*, 8513–8523.

(5) Kirby, A. J.; Hollfelder, F. *From Enzyme Models to Model Enzymes*; RSC Publishing: Cambridge, 2009.

(6) (a) Menger, F. M. *Pure Appl. Chem.* **2005**, *77*, 1873–1886. (b) Yunes, S. F.; Gesser, J. C.; Chaimovich, H.; Nome, F. *J. Phys. Org. Chem.* **1997**, *10*, 461–465. (c) Bruice, T. C.; Lightstone, F. C. *Acc. Chem. Res.* **1999**, *32*, 127–136. (d) Hur, S.; Bruice, T. C. *Proc. Natl. Acad. Sci. U.S.A.* **2003**, *100*, 12015–12020.

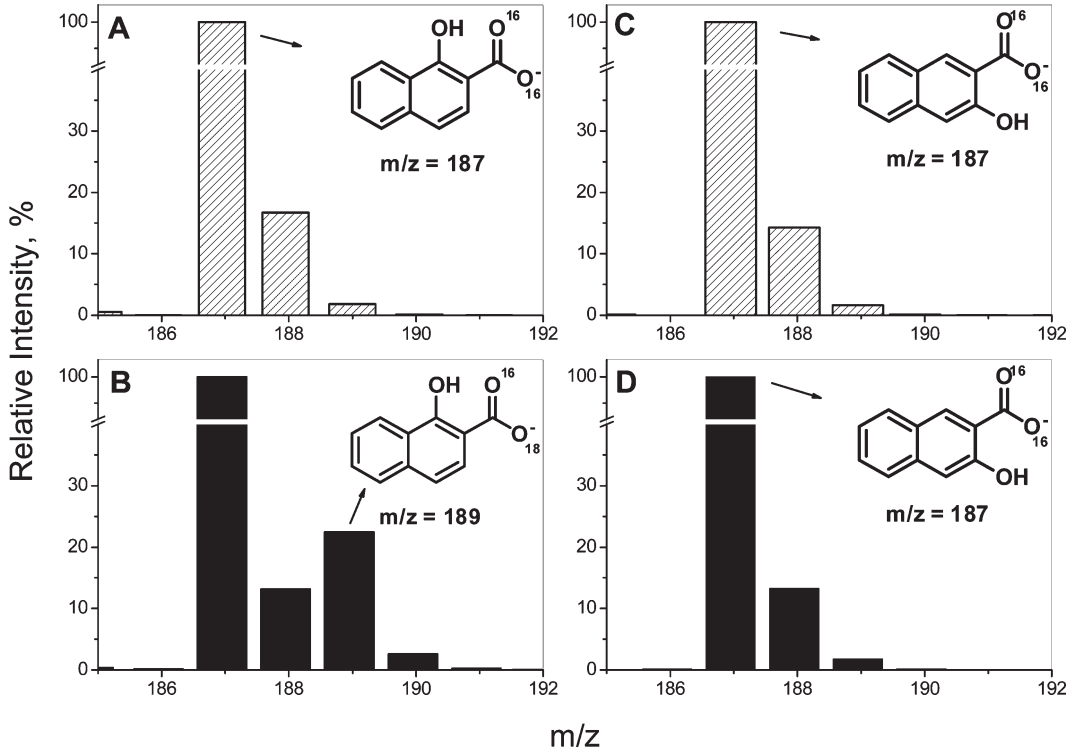

FIGURE 2. ESI-MS data for hydrolysis products of **1AC2NA** in (A) H_2O and (B) 20% ^{18}O-labeled water. Corresponding data for hydrolysis of **3AC2NA** in (C) H_2O and (D) 20% ^{18}O-labeled water. Arrows indicate m/z 187 and 189 peaks. The full m/z scale is shown in Figures S1 and S2 in Supporting Information.

TABLE 1. Kinetic Data for Hydrolyses of 1AC2NA and 3AC2NA at 45 °C and μ = 1 M (KCl)

ester	pK_a	$10^4 \times k_{H^+}$ (M^{-1} s^{-1})	k_{OH^-} (M^{-1} s^{-1})	$10^4 \times k_a$ (s^{-1})	$10^4 \times k_b$ (s^{-1})
1AC2NA	2.79	0.29	0.17	0.04	0.80
3AC2NA	3.43	1.55	0.77	0.01	0.15

For both compounds, k_b is the first order rate constant for hydrolysis in the pH-independent region (region iii in Figure 1) and k_a is the first order rate constant for the minor contribution of the COOH form (region ii in Figure 1), k_{H^+} and k_{OH^-} are the usual second order rate constants for specific acid and base catalysis whose major contributions are in regions i and iv, respectively, and K_a is the acid dissociation constant of the corresponding *o*-acetoxynaphthoic acid. The initial products are acetic acid/acetate and the corresponding 1-hydroxy-2-naphthoic (**1OH2NA**) and 3-hydroxy-2-naphthoic (**3OH2NA**) derivatives. In the acid region, the initially formed **1OH2NA** slowly decomposes to form 1-naphthol, identified by comparison with an authentic standard.

Table 1 shows the derived rate constants and pK_a's obtained from the pH−rate profile by using eq 1. In both compounds, both carboxyl and carboxylate groups catalyze ester group hydrolysis, showing a behavior qualitatively similar to that observed for aspirin.[2c] Hydrolysis of the anion (k_b) is 20 and 15 times faster than those of the neutral forms (k_a) for **1AC2NA** and **3AC2NA**, respectively.

We note that rate constants k_{H^+} and k_{OH^-} for the respective specific acid and base catalysis for hydrolyses of **3AC2NA** are about 5.3- and 4.5-fold greater, respectively, than the corresponding rate constants for hydrolysis of **1AC2NA**. Conversely, for the water reaction, the reactivity of **1AC2NA** is 4- to 6-fold greater than that of **3AC2NA**, both in the anionic (k_b) and neutral forms (k_a).

While the rate constants in the specific acid and base catalysis regions are not surprisingly different from those reported for the salicylic acid reaction, the inversion of reactivity observed in the water reaction is unexpected and indicates a change in mechanism, especially because there is a minor change in the spatial relations between the neighboring carboxylic and acetoxy groups.

The values of k_{obs} (= k_b) in the pH-neutral plateau region (around region iii in Figure 1) are considerably higher than for the hydrolysis of phenyl acetate,[7] and we focused our studies on the mechanism of hydrolyses of the anionic forms of the esters, which given the shapes of the pH−rate constant profiles in the plateau region could involve either nucleophilic or general base catalysis. Because the two mechanisms are kinetically undistinguishable, we examined in the pH-independent plateau region the hydrolyses of **1AC2NA** and **3AC2NA** in D_2O and in 20% $H_2{}^{18}O$.

Isotopic Labeling, Kinetic Isotope Effect and Thermodynamic Parameters. Hydrolyses of **1AC2NA** and **3AC2NA** in ^{18}O-labeled water were examined as described elsewhere,[2a] and products were analyzed by ESI-MS in negative mode with H_2O/CH_3CN 1:9 as mobile phase. The same procedure was followed in H_2O for comparison, and the data are given in Figure 2.

Figure 2 shows the ratio of intensities of the M + 2 (m/z 189) and M (m/z 187) peaks, relative to those in samples with

(7) Kirby, A. J.; Lloyd, G. J. *J. Chem. Soc., Perkin Trans 2* **1976**, 1753–1761.

SCHEME 4. Proposed Mechanisms Showing (*i*) Nucleophilic Intramolecular Attack in 1AC2NA with Incorporation of ^{18}O in 1OH2NA and (*ii*) General Base Catalysis for 3AC2NA, with Incorporation of ^{18}O in the Acetic Product; *O Indicates ^{18}O

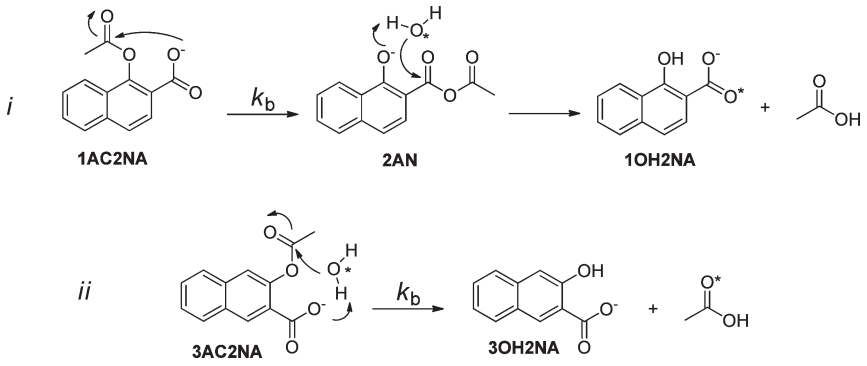

TABLE 2. Kinetic Isotope Effects and Activation Parameters for Hydrolyses of 1AC2NA and 3AC2NA and Labeled Oxygen Incorporation into Products 1OH2NA and 3OH2NA at pH 6.5 (Phosphate Buffer, μ = 1.0 M)

	1AC2NA	3AC2NA
% ^{18}O incorporation[a]	20	0
k_{H_2O}/k_{D_2O}[b]	1.16	2.42
$\Delta G^{\ddagger}$ at 25 °C (kcal mol^{-1})[c]	26.48	27.06
$\Delta H^{\ddagger}$ (kcal mol^{-1})[d]	27.19 ± 0.97	19.27 ± 0.48
$\Delta S^{\ddagger}$ (cal mol^{-1} K^{-1})[e]	3.3 ± 2.4	−26.1 ± 1.6

[a]Calculated from the differences in the *m*/*z* 189 peak for hydrolyses in natural vs 20% ^{18}O-labeled water. [b]Values are ±3%, at 45 °C. [c]Estimated using $\Delta G^{\ddagger} = RT \ln[(k_B T)/(hk_b)]$, where k_B and h are the Boltzmann and Planck constants, respectively, k_b is taken from the Eyring plot at 25 °C, and T is the temperature. [d]Obtained from the Eyring plot given in Figure S3 in Supporting Information. [e]Estimated using $\Delta G^{\ddagger} = \Delta H^{\ddagger} - T\Delta S^{\ddagger}$, at 25 °C.

natural abundance, thereby providing information on the extent of incorporation of $H_2{}^{18}O$ into the products of the hydrolyses of **1AC2NA** (Figure 2A and B) and **3AC2NA** (Figure 2C and D). Clearly, the two esters exhibit dramatically different behavior, as summarized in Table 2. Comparing panels A and B of Figure 2, it can be clearly seen that in the hydrolysis of **1AC2NA** a large increase in the M + 2 peak is observed in the reaction conducted in ^{18}O-enriched water; this large increase allowed us to calculate the incorporation of ^{18}O in **1OH2NA** given in Table 2. Conversely, panels C and D of Figure 2 show basically identical M and M + 2 peaks for **3OH2NA**, showing that ^{18}O is not incorporated in the hydrolysis of **3AC2NA**. Also included in Table 2 are solvent hydrogen kinetic isotope effects (k_{H_2O}/k_{D_2O}) and activation parameters for both hydrolyses in the plateau region (pH 6.5).

In the case of **3AC2NA** hydrolysis, the solvent ^{18}O isotopic labeling results are fully consistent with a mechanism involving general base catalysis where no labeled oxygen is incorporated into the product, **3OH2NA**. As expected from the proposed general base catalysis, ^{18}O isotopic labeling for the hydrolysis of **3AC2NA** showed incorporation of ^{18}O into the acetate anion product. By contrast, the isotopic labeling results for the hydrolysis of **1AC2NA** are fully consistent with a mechanism involving nucleophilic attack. In fact, the incorporation of labeled oxygen into the **1OH2NA** product is compelling evidence for the formation of the anhydride intermediate **2AN** (Scheme 4) in the hydrolysis of **1AC2NA** in the plateau region. That is, the **1AC2NA** reaction proceeds *via* nucleophilic catalysis without incorporation of ^{18}O in the acetate anion. Taken together, the results presented in Figure 2 show that these apparently similar esters are hydrolyzed through very different mechanisms. The activation parameters are those expected for the proposed mechanistic routes, showing a small positive entropy of activation for the intramolecular reaction of **1AC2NA** (route i in Scheme 4) and a larger and negative entropy of activation for the general base mechanism proposed for the **3AC2NA** ester (route ii in Scheme 4).[2a,b]

The small kinetic isotope effect, k_{H_2O}/k_{D_2O} = 1.16, coupled with the quantitative incorporation of ^{18}O in the reaction product from **1AC2NA**, demonstrates the nucleophiIic catalysis pathway, thus ruling out a general base mechanism with participation of water as a reactant in the rate-limiting step. The absence of a solvent hydrogen isotope effect shows that attack of water in the second step of reaction i in Scheme 4 must be fast relative to anhydride formation. The ^{18}O incorporation indicates that in the reaction of **1AC2NA** the attack of water on the anhydride intermediate must occur almost exclusively at the carbonyl group that is bonded to the aromatic ring given that the content of ^{18}O in the solution is 20%. Because in related compounds, such as acetic benzoic anhydride, there is only 25% attack at the aromatic carbonyl carbon, the results show that general base assistance by the neighboring phenolate generated in the first step plays an important role, favoring attack on the aromatic carbonyl center. Since protonation of **2AN** anion should proceed readily under the experimental conditions, general acid catalysis could also contribute to favor the regioseletive water attack. The observed kinetic isotope effect in the hydrolysis of **3AC2NA**, k_{H_2O}/k_{D_2O} = 2.42, is typical of reactions proceeding via general base catalysis; this kinetic isotope effect is also consistent with the incorporation of ^{18}O into the acetate product (reaction ii in Scheme 4).

This mechanistic divergence cannot be explained in terms of simple electronic effects because the second pK_a's of **1OH2NA** and **3OH2NA** (about 13.0 and 12.5, respectively, obtained by titration; see Figures S4 and S5 in Supporting Information) are not significantly different. Presumably significant ground state differences in **1AC2NA** and **3AC2NA** control the different mechanisms.

Computational Calculations. On this basis, we constructed the relaxed potential energy surface (RPES) for anionic **1AC2NA** and **3AC2NA** at the B3LYP/6-31+G(d) level, locating all conformations associated with rotations of the

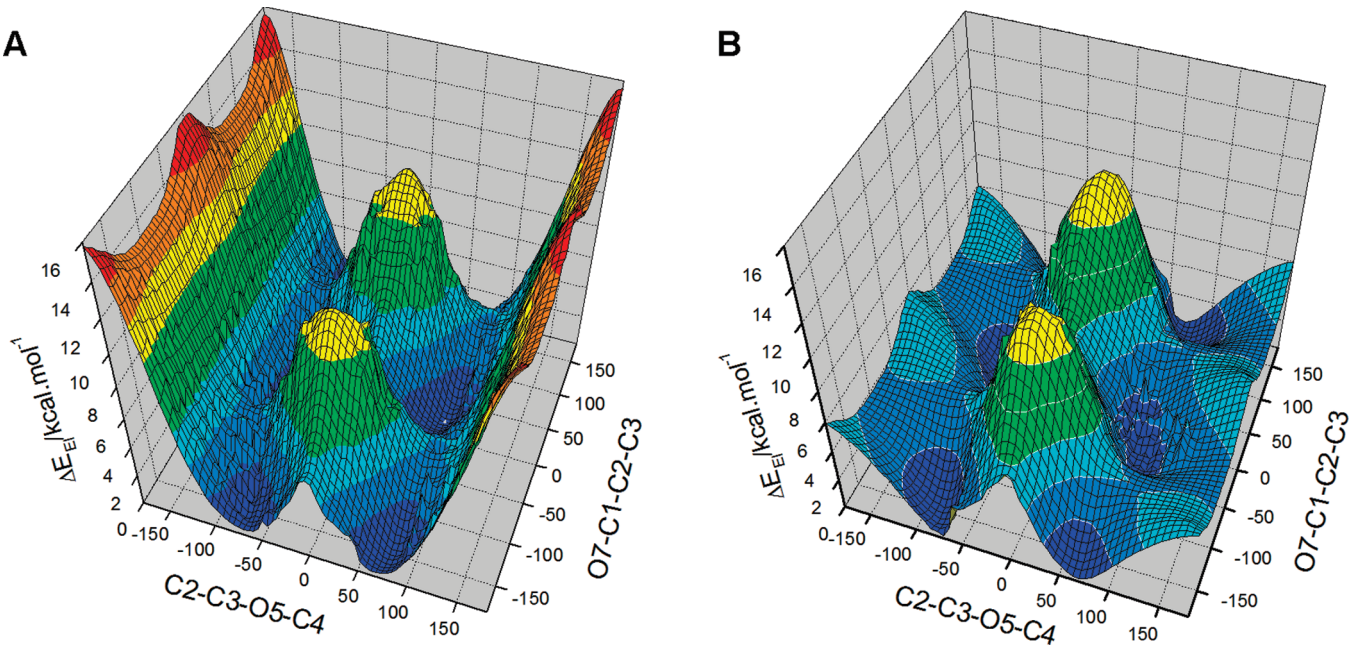

FIGURE 3. B3LYP/6-31+G(d) relaxed energy potential surface for the anionic (A) **1AC2NA** and (B) **3AC2NA** obtained by twisting the ester and carboxylate groups relative to the aromatic mean plane. Numbering is according to Scheme 5.

SCHEME 5. Geometrical Features and Numbering Used To Construct the RPESs Shown in Figure 3; Arrow Indicates the 8-Hydrogen in 1AC2NA

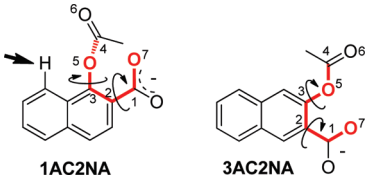

ester and carboxylate groups relative to the mean aromatic ring plane (Scheme 5). We refer to the RPES because every point in the 3D grid represents an optimized structure in which two dihedral angles are frozen, while all other bond distances, angles, and dihedrals were set free in order to obtain local minima. The results are in Figure 3 and show the energy costs for rotation of the reactive groups.

The RPES shows that in **3AC2NA** the maximum energy conformer has a relative energy of about 12 kcal mol^{-1} and is located in the plane where the C2−C3−O5-C4 dihedral angle is about 0° as a result of the repulsive interaction between the carboxylate and ester groups, with the latter coplanar to the aromatic ring. Besides this unfavorable interaction, all other conformers are within a few kilocalories, and 75% of the energy map contains structures within 5 kcal mol^{-1} of the most stable conformer, so that the ester group rotates almost freely. Conversely, in **1AC2NA**, as well as a similar maximum energy conformer in the plane of the C2−C3−O5−C4 dihedral angle of 0°, there is a high barrier associated with angles higher than 150° for the ester/ring dihedral. Thus, the ester group does not rotate freely and only 48% of the map is populated by structures within 5 kcal mol^{-1} energy. This high energy wall is structurally associated with *peri*-interactions with the 8-hydrogen (see arrow in Scheme 5), which acts as a bumper, pushing back the ester group. Thus, in **1AC2NA**, the ester group is pushed toward the carboxylate group, and the reactive groups are forced to reside longer in a conformation suitable for intramolecular nucleophilic attack. It is interesting to note that the global minima structures of **1AC2NA** and **3AC2NA** show suitable conformations for intramolecular nucleophilic attack (Figure 4 and geometrical parameters given in Table 3) and the most stable conformers have adequate conformations to be the more reactive ones.[6a−c] In these structures, the O7−C4 distance is 2.67 and 2.66 Å and the O7−C4−O6 angle is 103.96° and 104.03° for **1AC2NA** and **3AC2NA**, respectively. Table 3 also presents the geometrical details of **1AC2NA** and **3AC2NA** optimized by using the polarizable continuum model (PCM) to mimic the water environment. As expected, on going from the gas phase to the polarizable continuum the carboxylate negative charge is stabilized, and there is a considerable increase in the O7−C4 distance. In addition the O7−C4−O6 angle deviates from the Bürgi−Dunitz angle, reflecting a poorer interaction between the carboxylate and the ester carbonyl groups. Nevertheless, when compared, both in gas and in the PCM phase, there is no major difference between **1AC2NA** and **3AC2NA** that would give key information regarding differences in the hydrolysis mechanisms of both esters. The crystal structure of the neutral acid **1AC2NA**[8] is qualitatively consistent with that calculated, especially in relation to the stereochemistry and distances between ester and carboxylic acid groups, as found for aspirin,[9] which is structurally similar to **3AC2NA**.

The most stable conformers of **1AC2NA** and **3AC2NA** show conformations that are strongly favorable for intramolecular nucleophilic attack. This observation is consistent with the experimental results obtained for the hydrolysis of **1AC2NA**; on the other hand, this observation undermines

(8) Souza, B. S.; Bortoluzzi, A. J.; Nome, F. *Acta Crystallogr., Sect. E* **2007**, *63*, O4523–U3325.
(9) Wilson, C. C. *New J. Chem.* **2002**, *26*, 1733–1739.

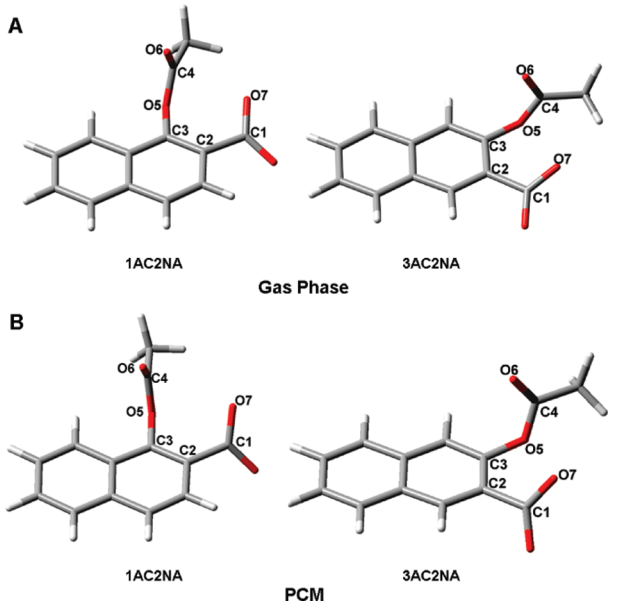

FIGURE 4. B3LYP/6-311++G(2df,p) global minima of **1AC2NA** anion and **3AC2NA** anion calculated in (A) the gas phase and (B) using the PCM to mimic the water environment. Main geometrical parameters are given in Table 3.

TABLE 3. Selected Distances and Angles for Optimized Structures of 1AC2NA and 3AC2NA Calculated at the B3LYP/6-311++G(2df,p) Level in the Gas Phase and by Using PCM To Mimic the Water Environment[a]

	1AC2NA		3AC2NA	
	gas phase	PCM[a]	gas phase	PCM[a]
O7−C4	2.69	2.99	2.68	3.10
O7−C1	1.25	1.25	1.25	1.25
O7−O5	2.75	2.88	2.74	2.91
O7−C4−O6	104.16	95.35	104.18	94.90
O7−C1−C2−C3	27.34	47.65	24.80	50.57
C2−C3−O5−C4	79.39	96.60	80.04	100.59

[a]Atomic radii obtained from the Simple United Atom Topological Model.

the IGBC mechanism observed for **3AC2NA**. A closer examination of the RPES shows that, for both esters, the most stable conformers show contact distances consistent with Menger's spatiotemporal hypothesis. This hypothesis states that reactions are fast when the reactive groups are held rigidly at a contact distance (less than the diameter of water, ca. 3 Å); thus, imposing time and distance constraints on two reactants necessarily brings them into proximity and speeds the reaction.[6a] In a sense, although the spatiotemporal concept does not account quantitatively for the experimental observations, it allows an initial qualitative analysis that is useful for understanding the differences in the mechanism for the two reactions being studied.

Dynamics of Conformer Equilibrium on the RPES. The RPES reveals that in both esters, **1AC2NA** and **3AC2NA**, high energy conformers with relative energies close to 12 kcal mol^{-1} arise from repulsive interactions between the carboxylate and ester groups, with the latter lying in the aromatic plane. Moreover, when the ester/ring dihedral is between 75° and 85° (C2−C3−O5−C4), the carboxylate group rotates freely, and the equilibria between the different structures proceed on a relatively flat potential energy surface. A detailed examination of the ~800 analyzed structures used to build the energy potential surface showed that in both compounds there was a probability of about 90% of the O7−C4 distance being between 2.4 and 3.0 Å. Statistical analysis of the O7−C4 distance showed that the distribution was slightly narrower for **1AC2NA** with full width at half-maximum (fwhm) of 0.22 Å, compared with a fwhm of 0.38 Å for the **3AC2NA** ester (see Supporting Information, Figures S6 and S7), a result consistent with the less restrained structure of **3AC2NA**.

The only significant difference between both compounds is the 13 kcal/mol^{-1} barrier associated with forcing the ester group to achieve angles higher than 150° for the ester/ring dihedral angle in the **1AC2NA** ester. This barrier should be compared with the small 3 kcal/mol barrier in **3AC2NA**, which allows the ester group to rotate almost freely from one side of the ring to the other. The dynamics of the process can be examined by considering rates of interconversion of acyclic conformers,[10] and considering $\Delta S \approx 0$ for the isomerization process, eq 2 can be used to estimate the interconversion constant k, where $\Delta H \approx \Delta E_{El}$ and is in calories per mole.

$$k = 2.084 \times 10^{10} T e^{-\Delta H/1.986T} \quad (2)$$

Equilibration of conformers via rotation of the acetoxi group on the direction from −80° → 0° → 80° favors the intramolecular reaction, since intercepts the actual reaction coordinate for nucleophilic attack, and the energy barrier is about 5.5 kcal mol^{-1} for both compounds, which corresponds to a rate of intercorversion of ca. 5.7×10^8 s^{-1} at 25 °C. Conversely, equilibration of conformers via rotation of the acetoxy group on the direction from −80° → −180° → 80°, for the **3AC2NA** isomer, needs to surpass a small barrier of 3.8 kcal mol^{-1} (see Figure 3B), which corresponds to a rate of interconversion (between conformers where the C2−C3−O5−C4 dihedral angle is about 80° to conformers with the same dihedral at −80°) of about 1.0×10^{10} s^{-1} at 25 °C. The equivalent rate for **1AC2NA**, which passes over a high energy wall (about 13 kcal mol^{-1}) due to the *peri*-interactions with the 8-hydrogen (vide supra), decreases to 7.7×10^3 s^{-1}.

Clearly, the dynamics of the equilibrium between conformers provides key insights to understand the difference in mechanisms. In the hydrolysis reaction of **1AC2NA**, the most stable conformer is in a conformation where there is not enough space to position a water molecule for a general base-catalyzed reaction to proceed. The dynamics of the nucleophilic reaction involves rotation of the acetoxy group in the direction −80° → 0° → 80°, thus intercepting the reaction coordinate for nucleophilic attack. Rotation in this direction proceeds with an interconversion rate of 5.7×10^8, which is 7.4×10^4-fold faster than the interconversion rate needed for a plausible water reaction (where rotation of the acetoxy group in the direction of the *peri*-hydrogen is needed to include a water molecule between the reacting groups), which requires overcoming a 13 kcal mol^{-1} wall, corresponding to a rate of 7.7×10^3 s^{-1}. Obviously, the nucleophilic reaction is highly favored by the energy wall. A similar analysis for the **3AC2NA** isomer shows that in the **3AC2NA** case, the reverse is true. It is less expensive in terms of energy

(10) Eliel, E. L.; Wilen, S. H.; Mander, L. N. *Stereochemistry of Organic Compounds*; Wiley: New York, 1994.

to move the acetoxy group, for the equilibration of conformers, via rotation in the direction $-80° \rightarrow -180° \rightarrow 80°$, with a small barrier of 3.8 kcal mol^{-1} and a rate of interconversion of 1.0×10^{10} s^{-1}, which is ca. 20-fold faster than the rate of interconversion in the direction $-80° \rightarrow 0° \rightarrow 80°$, which as described above favors the nucleophilic attack. Rotation in the direction $-80° \rightarrow -180° \rightarrow 80°$ increases the distance between the reacting groups and helps to position a water molecule in the correct conformation for the general base catalysis reaction.

Conclusions

These closely related compounds show how subtle structural differences may lead to major changes in reaction mechanism that, although kinetically equivalent, could be distinguished by means of isotopic labeling, kinetic isotope effects, and activation parameters. Such differences in mechanisms are certainly present in many enzymatic reactions, where reaction mechanism may well be controlled by conformational effects, which are optimized to have an appropriate time window for the reaction to proceed. In the reaction of the conformationally unrestrained 3-acetoxy compound, there is intramolecular general base catalysis. Conversely, for the 1-acetoxy derivative, a conformational constraint due to *peri*-interactions forces the reacting carboxylate and ester pair to remain longer in conformations that favor a reaction route proceeding via intramolecular nucleophilic attack. The results highlight the importance of the role of the dynamics of equilibrium between most stable conformers in the control of the reaction mechanism, (i) promoting the nucleophilic attack in **1AC2NA** by allowing the most stable conformers to equilibrate only via rotation in a direction that intercepts the reaction coordinate and (ii) favoring a general base-catalyzed water attack in **3AC2NA** by favoring equilibration via rotation that allows inclusion of a water molecule in a proper position for reaction.

Experimental Section

Materials. 1-Acetoxy-2-naphthoic acid (**1AC2NA**) was prepared by a procedure similar to that reported by Bergeron et al.[11] Concentrated sulfuric acid (10 drops) was added to a refluxing mixture of 1-hydroxy-2-naphthoic acid (3.50 g, 18.6 mmol) in acetic anhydride (8 mL, 89.7 mmol). The mixture was kept under reflux for 10 additional minutes, and after cooling to room temperature, the pale solid was filtered off and recrystallized in aqueous ethanol. The pale crystals melt at 138−139 °C. ^{1}H NMR (400 MHz, acetone-d_6, TMS): δ 8.16 (1H, d, J = 8.26); 8.07 (1H, d, J = 8.67); 8.03 (1H, d, J = 7.97); 7.91 (1H, d, J = 8.67); 7.70 (1H, t, J = 7.43); 7.65 (1H, t, J = 7.65), 2.46 (3H, s). ν_{max} (KBr) 3080−2600, 1766, 1683, 1296, and 1207 cm^{-1}. m/z (ESI-MS, negative mode, mobile phase H_2O/CH_3CN 1:9): 270 (4,60%, M − H + CH_3CN), 229 (32,5%, M − H), 187 (100%, M − CH_3CO). The isomer 3-acetoxy-2-naphthoic acid (**3AC2NA**) was prepared following the same procedure used to prepare **1AC2NA** using 3-hydroxy-2-naphthoic (**3OH2NA**) acid instead of 1-hydroxy-2-naphthoic acid (**1OH2NA**). Slightly yellow crystals, mp 183−184 °C. ^{1}H NMR (400 MHz, acetone-d_6, TMS): δ 8.69 (1H, s); 8.11 (1H, d, J = 8.12); 7.97 (1H, d, J = 8.17); 7.68 (2H, m); 7.61 (1H, t, J = 7.37), 2.30 (3H, s). ν_{max} (KBr) 3084−2800, 1764, 1700, 1294, 1207 cm^{-1}. m/z (ESI-MS, negative mode, mobile phase H_2O/CH_3CN 1:9): 270 (17.80%, M − H + CH_3CN), 229 (25%, M − H), 187 (100%, M − CH_3CO). The complete FTIR, ESI-MS, and ^{1}H NMR (400 MHz, acetone-d_6) spectral data for both **1AC2NA** and **3AC2NA** are given in Supporting Information.

Kinetics. Reactions followed spectrophotometrically were started by adding 20 μL of a stock solution of the substrate (0.01 M in acetonitrile) to a buffered aqueous solution (3 mL) at the appropriate pH. Kinetics were followed, at constant temperature and ionic strength 1.0 M (KCl), for at least five half-lives, by monitoring the appearance of **1OH2NA** (344 nm for pH values smaller than 3.40 and 314 nm for pH values higher than 3.40) or **3OH2NA** (350 nm) on a spectrophotometer equipped with a thermostatted cell holder. Activation parameters were calculated by using the Eyring equation from rate constants at pH 6.65 (phosphate buffer, 0.01 M, μ = 1.0M). The pH values of the reaction mixtures were measured at the end of each run. Observed first order rate constants (k_{obs}) were calculated by nonlinear least-squares fitting of the absorbance versus time; correlation coefficients were 0.998 or better. Buffers were HCl/KCl (pH ≤ 2), chloroacetate (pH 2.0−3.5), formate (pH 3.0−4.0), acetate (pH 4.0−5.5), phosphate (pH 5.5−7.0), bis-TRIS (pH 7.0−9.0), carbonate (pH 9.5−11.0), and NaOH (pH ≥ 12). Data from kinetic measurements are summarized in Tables S1−S2 in Supporting Information. The solvent isotope effect was calculated from the ratio of k_{obs} in H_2O and D_2O in phosphate buffer at pH 7.0 or pD = 7.3,[12] μ = 1.0 M (KCl), and 45 °C.

Labeling Experiments. Hydrolysis of **1AC2NA** and **3AC2NA** in the presence of ^{18}O-isotope labeled water was performed as described elsewhere.[2a] A 1-mL glass ampule containing 5 mg of **1AC2NA** or **3AC2NA**, 82 mg of sodium acetate, 0.2 mL of THF, 0.1 mL of HCl 1 M, and 0.6 mL of 20 atom % enriched $H_2{}^{18}O$ was sealed and incubated at 45.00 °C for $5t_{1/2}$ (at pH 5.00). The products were analyzed by ESI-MS in negative mode using H_2O/CH_3CN 1:9 as mobile phase, and the reaction was also carried out in unlabeled water following the same procedure with no significant m/z 189 peak.

Mass Spectrometry. Mass spectroscopic identifications were performed in a low-resolution instrument with the direct injection mode of 10^{-5} M sample solutions as carried out in other studies.[13] The interface, CDL, and block temperatures were set at 250, 250, and 200 °C, respectively. The detector was maintained at 1.50 kV, the flow of N_2 was 1.5 L min^{-1}, and the mobile phase was 1:9 H_2O/CH_3CN

NMR Spectroscopy. All ^{1}H spectra were monitored at 400 MHz, 25 °C, in acetone-d_6. The ^{1}H chemical shifts are referred to internal TMS.

Computational Methods. All computational calculations were performed using Gaussian 03[14] at the DFT level employing the hybrid B3LYP[15] functional. Global minima structures were optimized using the 6-311++G(2df,p) basis set and properly characterized in force constant calculations by the absence of a single negative eigenvalue. The construction of the RPESs was performed using the 6-31+G(d) basis set using the "*Scan*" keyword, which requests that a potential energy surface (PES) scan be done over a rectangular grid involving selected internal coordinates. The selected variables were the mean ring plane/ester

(11) Bergeron, R. J.; Wiegand, J.; Wollenweber, M.; McManis, J. S.; Algee, S. E.; Ratliff-Thompson, K. *J. Med. Chem.* **1996**, *39*, 1575–1581.

(12) Fife, T. H.; Bruice, T. C. *J. Phys. Chem.* **1961**, *65*, 1079–1080.

(13) Kirby, A. J.; Medeiros, M.; Oliveira, P. S. M.; Brandao, T. A. S.; Nome, F. *Chem.—Eur. J.* **2009**, *15*, 8475–8479.

(14) Frisch, M. J., et al. *Gaussian 03*, revision D.01; Gaussian, Inc.: Pittsburgh, PA, 2004.

(15) (a) Becke, A. D. *J. Chem. Phys.* **1993**, *98*, 5648–5652. (b) Stephens, P. J.; Devlin, F. J.; Chabalowski, C. F.; Frisch, M. J. *J. Phys. Chem.* **1994**, *98*, 11623–11627. (c) Vosko, S. H.; Wilk, L.; Nusair, M. *Can. J. Phys.* **1980**, *58*, 1200–1211. (d) Lee, C. T.; Yang, W. T.; Parr, R. G. *Phys. Rev. B* **1988**, *37*, 785–789.

dihedral angle and the mean ring plane/carboxylate dihedral angle as defined above. The calculations were performed using the "*Loose*" keyword in order to achieve local minima structures, with an step size of 8°. Relative energies were calculated from the electronic energies differences (ΔE_{El}).

Spectrofluorimetric Titration. The spectrofluorimetric titration of 1-hydroxy-2-naphthoic acid (**1OH2NA**) and 3-hydroxy-2-naphthoic acid (**3OH2NA**) were performed at room temperature, by measuring the emission intensity at 318 and 312 nm, respectively, of a 66.6 μM solution of the hydroxy acids. The pH was changed by addition of small aliquots of HCl or KOH 1 M from pH 2.00 to 12.00, and the intensity was corrected by the dilution factor. Above and under pH 2.00−12.00, standard KOH or HCl solutions were used, and the ionic strength was kept constant (1.0 M) by addition of KCl. Results are given in Supporting Information, Figures S4 and S5.

Acknowledgment. We are grateful to INCT-Catálise, PRONEX, FAPESC, CNPq and CAPES for support of this work and to Professor Ricardo L. Longo for its help in constructing the RPES.

Supporting Information Available: Characterization of **1AC2NA** and **3AC2NA**, kinetic details, titration curves of **1OH2NA** and **3OH2NA**, 2D plots of the RPESs, Cartesian coordinates of **1AC2NA** and **3AC2NA**, and Gaussian full reference. This material is available free of charge via the Internet at http://pubs.acs.org.